Int. J. Electrochem. Sci., 13 **(2018)** 822 – 831, doi: 10.20964/2018.01.77

International Journal of ELECTROCHEMICAL SCIENCE
www.electrochemsci.org

Short Communication

Electrodeposition of a YSZ–Yttria Stabilized Zirconia Composite Coating on a Titanium Bone Implant

Xin Yin[1], *Cunfu Liang*[2,*] *and Fengxiao Ge*[1]

[1] Department of Arthrosis surgery, Linyi People's Hospital, Linyi City, Shandong Province, 276000, P.R. China
[2] Department of General Medicine, Linyi People's Hospital, Linyi City, Shandong Province, 276000, P.R. China
[*]E-mail: liangcunfu_vip@sina.com

Received: 17 September 2017 / *Accepted:* 19 November 2017 / *Published:* 16 December 2017

For load-bearing or bone-contacting applications, including renovation of congenital skeletal abnormalities, joint and tooth replacement, and fracture healing, metallic implants have gained extensive use and acceptance. Cathodic electrodeposition from zinc sulfate-based electrolytes containing gelatin was carried out to prepare composite coatings of zinc and nano-sized yttria-stabilized zirconia (YSZ) particles. Through immersion in simulated body fluid and cell proliferation performed separately several times, the apatite precipitation of the YSZ-coated Ti was studied to measure its biocompatibility and bioactivity. It can be seen that the developed YSZ-Ti showed decreased inflammatory response compared to bare Ti implants due to its excellent tissue attachment features, apatite formation capacity, and biocompatibility.

Keywords: Electrodeposition; Yttria stabilized zirconia; Coating; Adhesion strength; Bone implant

1. INTRODUCTION

Metallic implants have been scientifically recognized and extensively applied as scaffolds in load-bearing or bone-contacting fields, including in tooth replacement, fracture healing, and renovation of congenital skeletal abnormalities [1-5]. In these metallic implants, commercially pure titanium (cpTi) and its alloys have excellent aesthetic and immunologic properties, thus being widely accepted as remarkable materials for use in oral implants for tooth substitutes [6-8]. Despite the excellent mechanical features and biocompatibility of Ti-based implants, they are still not suitably durable for applications in which implants must endure corrosive environments, such as in body fluid, over long periods[1]. Several drawbacks of Ti result from contact with fluoride and saliva, including galvanic side effects, inflammatory response, and allergic reactions [9-12]. These effects suggest that surface

modification, wherein a bioactive and protective coating is generated, could enhance the suitability and sustainability of Ti implants under physiological conditions [13-15]. Ti implants show bone-bonding capacity upon the application of a bioactive hydroxyapatite (HA) coating onto the Ti surface [16-18]. Unfortunately, Ti implants with a normal HA coating still suffer some drawbacks, including undesirable densification, lack of adhesion, and cracks, which result from the irregular interparticle spacing, thermal stress, etc. [19, 20]. Moreover, upon exposure to fluoride and saliva under corrosive conditions in the oral environment, the HA coating would not last due to its poor chemical inertness. These results indicate that many different problems from use of the aforementioned HA coating would arise after implantation due to its undesirable chemical inertness and mechanical properties, including corrosion, fast dissolution, delamination, deficiency in osteoconductivity, and implant-associated infections brought on by bacterial colonization [21, 22].

Zirconia (ZrO_2) has desirable appearance, chemical inertness, bone-bonding ability, thermal stability, and fracture toughness properties, thus having been recognized as a useful ceramic material in the biomedical field [23-25]. Under ambient pressure and temperature, pure ZrO_2 shows allotropic and polymorphic properties, with the following three crystallographic shapes: cubic, monoclinic, and tetragonal [26]. Cubic ZrO_2 shows the highest stability and has distinct functional and constructional features, including high mechanical strength, erosion and alkali resistance, thermal insulation, ability to prevent crack propagation, and wear resistance [27]. Furthermore, it could enhance the bonding between the implant and surrounding living tissues due to its remarkable biocompatibility [28], non-cytotoxicity [29, 30], and moderate bioactivity [31]. ZrO_2 has gained substantial attention as an excellent material for prosthetic dentistry, considering its ability to promote implant osteoconductivity and reduce bacterial colonization [32]. Research has confirmed that the deposition of cubic ZrO_2 on the Ti surface as nanocoating brought minimized inflammatory response to the oral replacements while promoting good anti-corrosion, biocompatibility, osseointegrativity, and anti-wear properties in the dental implants [33]. Magnetron sputtering and plasma spray deposition have been reported as methods for developing pure ZrO_2 or ZrO_2-based composite coatings on Ti/Ti-alloy implants [34, 35]. Unfortunately, a majority of the formed coatings showed inhomogeneity, poor thickness and adhesion, and proneness to cracks [36, 37]. However, no studies have reported on the biological characterization of these coatings. Additionally, many different complications remain in terms of the formation of this crystalline uniform coating on the surface of Ti with appropriate adhesion and hardness. *In situ* development of ZrO_2 nanocrystals on the metal surface is required to obtain desirable crystallinity and phase, as well as more favorable mechanical properties. This process necessitates heat-treatment of the coated samples at a relatively high temperature [38, 39]. In this annealing process, oxidization, contamination, or thermal deterioration would occur to Ti, which could lead to depreciated mechanical strength, chemical properties, and biological responses.

In the present study, a YSZ–yttria-stabilized zirconia composite coating was prepared with an electrolyte additive of gelatin via electrodeposition to develop a highly efficient and chemically inert oral implant using crystalline ZrO_2. Using cpTi (Z-cpTi), the formed fine-crystalline cubic ZrO_2 nanocoating showed remarkable homogeneity and adhesion. With the use of this simple and appealing synthetic approach, the crystalline cubic ZrO_2 nanocoating developed on Ti metal exhibited

desirable bioactivity, biocompatibility, and hardness. Detailed information on the primary cellular response and apatite formation capacity of Z-cpTi is also presented.

2. EXPERIMENTS

2.1. Chemicals

All reagents were used as received. Zirconium(IV) *n*-propoxide (ZP) in *n*-propanol (70%) was commercially available from Alfa Aesar. 1-Butanol, acetylacetone (acac),1-Propanol, and nitric acid were commercially available from Sigma. Commercially pure titanium (grade 4, 99% pure) was employed for coating as metallic dental implants.

2.2. Electrodeposition

Electrodeposition measurements were carried out in a zinc sulfate-based electrolyte solution that contained YSZ (8%; surface area, 7 m^2/g; TOSOH) and gelatin (MW = 60,000, Norland) at ambient temperature. The solution pH was adjusted by a sulfuric acid solution (10 vol.%). Cathode substrates of commercially pure titanium (grade 4; 99% pure; dimensions, 50 mm × 50 mm × 0.1 mm) were placed between two 99.99% pure zinc anodes (dimensions, 60 mm × 50 mm × 1 mm). For the electrodeposition measurements, the deposition time and constant current density were 20 min and 20 mA/cm^2. The stirring speed for the electrolytes was 300 rpm during all deposition processes. Titanium substrates were electrodeposited, followed by degreasing at room temperature with a sodium hydroxide solution (2 vol.%), rinsing using deionized water, 20 min of ultrasonic cleaning in isoproponal, rinsing using acetone, and drying in a warm air stream.

2.3. Characterizations

A Bruker D8 powder X-ray diffractometer was used to obtain X-ray diffraction (XRD) patterns, scan rate: 0.5 °/min. The ratio *R* of the relative intensities *I* of XRD reflections of the basal (0002) and pyramidal planes (1011) was used for analysis of the preferred orientation of the deposits. A LECO M-400-H2 microhardness testing machine (load, 10 g) was employed to measure Vickers microhardness of the YSZ deposits. A three-electrode cell-equipped PARSTAT 2273 (Princeton Applied Research) electrochemical system was used for potentiodynamic polarization measurements, where the counter and reference electrodes were a platinum mesh and a saturated calomel electrode (SCE), respectively. Examination of pure zinc and composite Zn–YSZ coatings was carried out in sodium chloride solution (5 wt.%), with a scan rate of 1 mV/s.

2.4 MTT assay analysis using MG63 cell line

MTT assays were performed on Zn–YSZ coatings with the pre-osteoblastic cell line MG63, derived from human osteosarcoma cells, to quantitatively investigate the cytotoxicity as well as the cell

proliferation and to visualize primary cellular response. The growth of viable MG63 cells attached on the sample surfaces after 3 and 5 d of incubation was measured by MTT assay, and for comparison, cells cultured on blank wells were used as a control. Three samples for each composition and two culture durations were used to evaluate cell proliferation. MTT solution [3-(4,5-dimethylthiazol-2-yl)-2,5-diphenyl tetrazolium] of 5 mg/mL concentration was prepared by dissolving MTT in PBS. Freshly prepared MTT solution was used for each assay which was also protected from light. MTT solution was diluted to 1 mg/mL with DMEM culture media enriched with 10% fetal bovine serum and added to each sample to form formazan salt through oxidation of tetrazolium by the action of the mitochondrial dehydrogenase enzyme. After 4 h of incubation at 37 °C, samples were transferred to a new 24-well plate, and 1 mL of solubilization solution (DMSO – dimethyl sulfoxide) was added to dissolve the formazan crystals. Then, 100 mL of the resulting supernatant was transferred into each well of a 96-well plate and at least three data points were obtained from each sample. The optical density of the solution in each well was measured at a wavelength of 570 nm using a microplate reader. The OD of wells containing only 100 mL of DMSO was measured as blank measurements.

3. RESULTS AND DISCUSSION

Solutions with and without 0.5–6 mg/L of gelatin and with varying pH were used to prepare YSZ coatings. The changes in gelatin concentration and pH brought changes to the relative intensities of the XRD peaks, as shown in the X-ray diffraction patterns in Figure 1A. The orientation of YSZ crystals in the coatings was significantly affected after adding gelatin into the electrolytes. In the deposits before adding gelatin (pH 3), a strongly preferred basal plane orientation was observed, as shown in the X-ray diffraction patterns (Figure 1A). These results confirmed that the basal plane preferred orientation is inhibited after adding gelatin into the deposition bath. In pH 5 and pH 3 electrolytes, the *R* ratio changes relative to the concentration of gelatin, as shown in Figure 1B. As the concentration of gelatin in the pH 3 electrolyte solution was increased over a range of 0 - 4 mg/L, a decrease in *R* was observed over a range of 6 - 0.5. As the concentration of gelatin was increased in the electrolyte solution, a decrease in the fraction of basal planes oriented parallel to the substrate surface was observed. These results showed that more randomly oriented YSZ crystals were formed after adding gelatin. On the other hand, coatings in the absence of gelatin at pH 5 showed a much decreased *R* relative to those at pH 3, which suggested that YSZ crystals in this solution were more randomly oriented. Therefore, crystallographic orientation was not significantly changed after adding gelatin into the pH 5 electrolytes.

The adsorption of gelatin onto a growing deposit surface was a possible reason for the effects of gelatin on the crystallographic orientation and morphology. Gelatin, a zwitterionic polymer, is a heterogeneous mixture of amino acids linked by peptide chains (–CO–NH–) and could be hydrolyzed. Gelatin also takes on a positive or negative charge, depending on the solution acidity. The protonation of amino groups on side chains under conditions lower than pH 4.5 contributed to the development of the positive charge on the gelatin molecules.

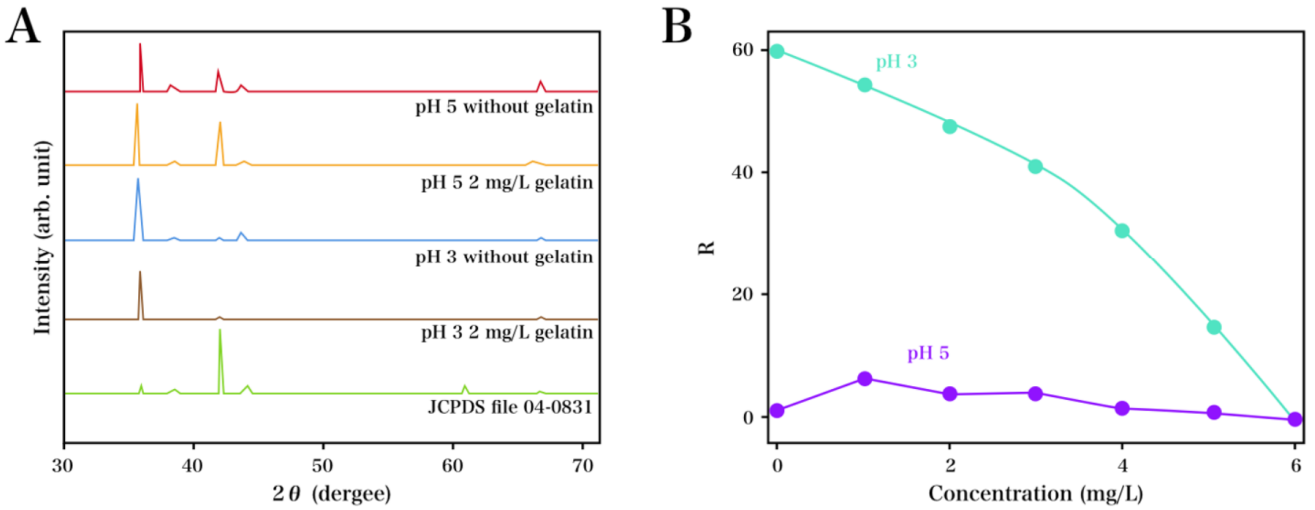

Figure 1. (A) XRD patterns recorded for the deposits prepared from $ZnSO_4$ solution: pH 5, in the absence of gelatin; pH 5, in the presence of 2 mg/L gelatin; pH 3, in the absence of gelatin; pH 3, in the presence of 2 mg/L gelatin and JCPDS file 04-0831. (B) XRD intensity ratio in solutions at pH 3 and pH 5.

The electrophoretic motion of charged gelatin onto the cathode surface was a suggested result from the electric field, and the adsorbed gelatin affected the deposition of YSZ. The adsorption of gelatin gave rise to a cathode overpotential increase, which further led to changed microstructure of the deposits.

The deposit microstructure was significantly changed after adding gelatin, which brought further hardness enhancement of the YSZ deposits. The relationship between the Vickers microhardness of the YSZ coatings and the concentration of gelatin in the electrolyte is shown in Figure 2. As the concentration of gelatin was increased from 0 to 3 mg/L, an increase in the microhardness of coatings was observed, which then reached a plateau upon further increase in the microhardness of gelatin. The possible reason for the increased microhardness was that the crystallographic orientation of the YSZ deposit was changed. The mechanical features could be significantly affected by the crystallographic orientation, which would indicate that the hexagonal crystal structure of YSZ results in its anisotropic mechanical features [40]. Deformation of hexagonal YSZ crystals was realized through slip on the (0001) basal planes [41]. YSZ crystals became more randomly oriented after adding gelatin, which decreased the fraction of basal planes parallel to the surface of the substrate. The results indicated that the orientation of the YSZ crystals increased the deposit microhardness by limiting basal plane slip.

It was shown that, under high overpotential, the deposit grew via outgrowth [42]. This behavior can be attributed to the redistribution of Zr^{2+} ions in the vicinity of the cathode surface in the electric field. An ion-deficient area would then form locally due to differences between the Zr^{2+} ion consumption rate at the electrode and the diffusion rate of Zr^{2+} ions from the bulk solution. The increase in cathode overpotential induced by gelatin adsorption expands this ion deficient area. Consequently, the growing tips of the deposit would encounter higher Zr^{2+} ionic concentrations than the lateral surfaces and would grow at a higher rate in the direction normal to the substrate surface.

Thus, in this experiment, the adsorption of gelatin promoted the formation of the observed ridge-shaped microstructure, which comprised zinc layers growing perpendicularly to the substrate surface.

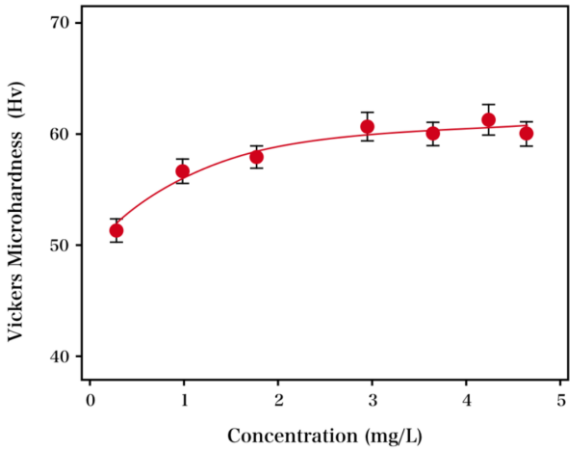

Figure 2. Microhardness of YSZ coatings versus the concentration of gelatin in pH 3 solution.

For the ceramic particles, the appropriate surface charge needed to be developed in order to deposit ceramic particles at the cathode, based on the electrophoretic deposition theory. Zeta potential corresponded to the particle surface charge, suggesting ceramic particle mobility. For YSZ, the point of zero charge (PZC) was obtained as *ca.* pH 6, indicating that positive zeta potential should be obtained when the pH is lower than 6. Results showed the development of positive charge on the surfaces of the ceramic particles under acidic conditions, as desired. However, dissolution of yttria occurred under acid conditions, which necessitated controlling the deposition solution pH within the moderate range. Particle charging and electrosteric stabilization could also be caused after protonated gelatin has been adsorbed onto the ceramic particle surfaces. It is therefore presumed that the co-deposition of ceramic particles was further enhanced after adding gelatin, possibly attributed to the following effects of gelatin on the co-deposition process: (1) the stabilizing effect on ceramic particle suspensions; (2) the morphology modification of pure YSZ deposits. For the YSZ deposits, a ridge-shaped microstructure was observed after adding gelatin into the experimental electrolytes, which increased the boundary area and the active sites for ceramic particle deposition. In this case, an increased number of ceramic particles was incorporated into the composite coating due to the changed morphology of the YSZ deposit. According to the electrophoretic deposition theory, the successful deposition of ceramic particles at the cathode requires the development of the appropriate surface charge on the ceramic particles. The representation of particle surface charge is the zeta potential, which determines the mobility of ceramic particles. In aqueous solutions, the zeta potential of YSZ versus pH was measured by Moreno et al. [43]. The point of zero charge (PZC) for YSZ was determined to be approximately pH 6. As the pH values in the present investigation were lower than 6, the zeta potential should be positive. Thus, in acidic solutions, the desired positive charge was developed on the ceramic particle surfaces. However, yttria dissolves in strongly acidic solutions, so the pH of the deposition solutions had to be controlled in the moderate range. It is also suggested that

the adsorption of protonated gelatin on the surface of ceramic particles can result in electrosteric stabilization and charging of the particles. Thus, it is suggested that the addition of gelatin further promoted the co-deposition of ceramic particles.

In vitro apatite forming ability is a typical property measured to evaluate the ability of bioactive coatings to support the implant bone-bonding capacity [44]. For comparison, the uncoated Ti plate was also employed as a control. After immersion for 14 d, island-like spherically shaped calcium phosphate deposition was found on the Z-cpTi [45]. However, on the control Ti, no precipitation was observed. On YSZ-Ti, precipitation was observed as shown in the XRD patterns in Figure 3A. The additional XRD peaks recorded for crystalline CO_3HA were consistent with the JCPDS card no. 01-075-3727. The main peak at $2\theta = 31.44°$ corresponded to the (121) plane of the CO_3HA phase. For the control Ti plates, no deposition of CO_3HA was observed, as shown in Figure 3B.

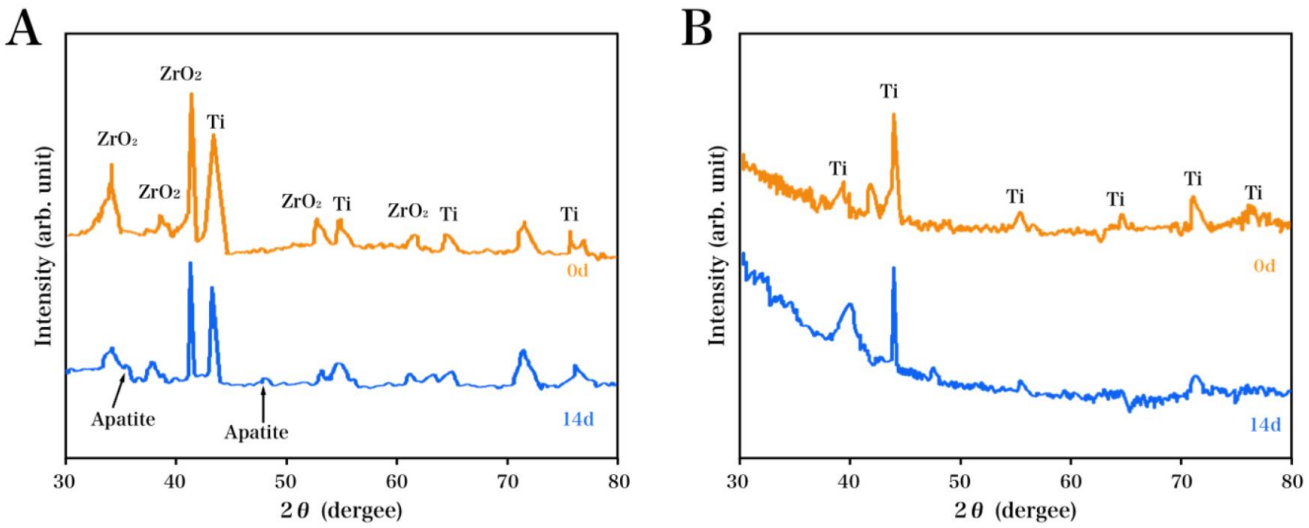

Figure 3. XRDs recorded for the (A) YSZ-Ti and (B) control Ti samples.

Human pre-osteoblastic MG63 cells, especially effective in assessing the biomaterial cytotoxicity that affects bone growth metabolism and cell–biomaterial interactions in bone tissue engineering, were used for MTT measurements in this study. The expression of the osteoblastic phenotype could be enhanced by bone tissue engineering materials by promoting activities such as cell proliferation and attachment. Figure 4 shows the quantitative analysis and comparison of the degree and biocompatibility of cell proliferation on the resulting ZSY-Ti and control Ti specimens after culturing for 3 and 5 d. Figure 4 also shows the plot of cell proliferation percentages *vs.* culture time in days, based on the obtained OD values. After 3 d, ZSY-Ti showed a better cell proliferation compared with that of the bare Ti, since the cells were primarily attached. After 5 d, the same tendency was observed. In the samples cultured for 5 d, our proposed ZSY-Ti showed higher cell proliferation than that of the control Ti, which indicated that the former material is highly biocompatible and noncytotoxic and possesses enhanced cell attachment ability.

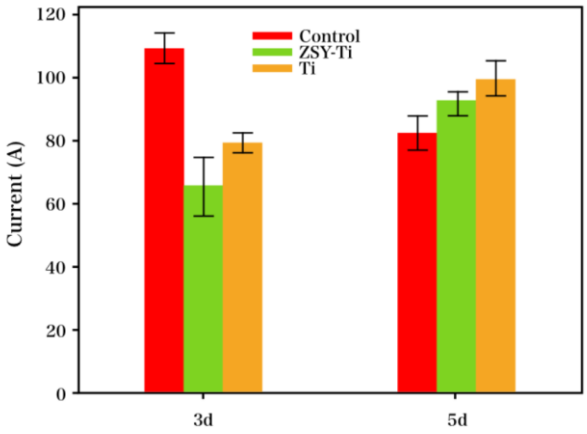

Figure 4. Percentage of MG63 proliferation during MTT measurement on the ZSY-Ti and reference Ti samples after 3 and 5 d of incubation.

4. CONCLUSIONS

For the preparation of Zinc/YSZ composite coatings, suspended YSZ particles were incorporated into a zinc sulfate electrolyte solution. The YSZ particles competed with Zn^{2+} ions for active deposition sites, which led to the preferential distribution of YSZ particles on the growing macrosteps and edges of the zinc deposit. Through the deposition of a crystalline YSZ nanocoating on the surface with no observable damage to the original metallic Ti features, this proposed synthetic route brought enhancement to the biological, chemical, and physical features of the implant. The chemically inert, novel nanostructure cubic YSZ coating brought osseointegration enhancement, along with a decrease in the inflammatory reaction of the metallic oral implants, due to its excellent bioactivity, including improved tissue attachment features, apatite deposition capacity, and biocompatibility.

References

1. W. Zhang, Z. Li, Q. Huang, X. Ling, J. Li, Y. Jin, G. Wang, X. Liu and X. Jiang, *International Journal of Nanomedicine*, 8 (2013) 257.
2. C.R. Arciola, L. Visai, F. Testoni, S. Arciola, D. Campoccia, P. Speziale and L. Montanaro, *International Journal of Artificial Organs*, 34 (2011) 771.
3. T.A. Hess, *Journal of Prosthetic Dentistry*, 112 (2014) 365.
4. B. Uzer, S.M. Toker, A. Cingoz, T. Bagci-Onder, G. Gerstein, H.J. Maier and D. Canadinc, *Journal of the Mechanical Behavior of Biomedical Materials*, 60 (2016) 177.
5. I. Das, S. Chattopadhyay, A. Mahato, B. Kundu and G. De, *Rsc Advances*, 6 (2016)
6. S.H. Oh, I.Y. Na and K.H. Choi, *Journal of Nano Research*, 23 (2013) 83.
7. A. Fritsche, F. Luethen, U. Lembke, B. Finke, C. Zietz, J. Rychly, W. Mittelmeier and R. Bader, *Materialwissenschaft Und Werkstofftechnik*, 41 (2010) 83.
8. H.J. Lee, J. Lee, J.T. Lee, J.S. Hong, B.S. Lim, H.J. Park, Y.K. Kim and T.I. Kim, *Journal of Periodontal & Implant Science*, 45 (2015) 120.
9. R. Willumeit, A. Möhring and F. Feyerabend, *International Journal of Molecular Sciences*, 15

(2014) 7639.
10. A. Alahmad, M. Wiedmannalahmad, A. Fackler, M. Follo, E. Hellwig, M. Bächle, C. Hannig, J.S. Han, M. Wolkewitz and R. Kohal, *Archives of Oral Biology*, 58 (2013) 1139.
11. M. Etxeberria, L. López-Jiménez, A. Merlos, T. Escuín and M. Viñas, *International Microbiology the Official Journal of the Spanish Society for Microbiology*, 16 (2013) 235.
12. K. Yamane, Y. Ayukawa, T. Takeshita, A. Furuhashi, Y. Yamashita and K. Koyano, *Clinical Oral Implants Research*, 24 (2013) 1310.
13. E.T.J. Rochford, A.H.C. Poulsson, J.S. Varela, P. Lezuo, R.G. Richards and T.F. Moriarty, *Colloids & Surfaces B Biointerfaces*, 113 (2014) 213.
14. E. Mohseni, E. Zalnezhad and A.R. Bushroa, *International Journal of Adhesion & Adhesives*, 48 (2014) 238.
15. E. Westas, L.M. Svanborg, P. Wallin, B. Bauer, M.B. Ericson, A. Wennerberg, K. Mustafa and M. Andersson, *Journal of Biomedical Materials Research Part A*, 103 (2015) 3139.
16. A. Arifin, A.B. Sulong, N. Muhamad, J. Syarif and M.I. Ramli, *Materials & Design*, 55 (2014) 165.
17. H. Daugaard, B. Elmengaard, J.E. Bechtold, T. Jensen and K. Soballe, *Journal of Biomedical Materials Research Part A*, 92 (2010) 913.
18. A. Thorfve, C. Lindahl, W. Xia, K. Igawa, A. Lindahl, P. Thomsen, A. Palmquist and P. Tengvall, *Acta Biomaterialia*, 10 (2014) 1451.
19. X. Liu, Y. Mou, S. Wu and H.C. Man, *Appl. Surf. Sci.*, 273 (2013) 748.
20. H.Y. Lin and S.L. Liao, *British Journal of Ophthalmology*, 95 (2011) 630.
21. Z. Cheng, C. Guo, W. Dong, F.M. He, S.F. Zhao and G.L. Yang, *Oral Surgery Oral Medicine Oral Pathology & Oral Radiology*, 113 (2012) e48.
22. C.M. Xie, X. Lu, K.F. Wang, F.Z. Meng, O. Jiang, H.P. Zhang, W. Zhi and L.M. Fang, *ACS applied materials & interfaces*, 6 (2014) 8580.
23. M. Le, E. Papia and C. Larsson, *Journal of Oral Rehabilitation*, 42 (2015) 467.
24. A. Zembic, A.O.H. Philipp, C.H.F. Hämmerle, A. Wohlwend and I. Sailer, *Clinical Implant Dentistry & Related Research*, 17 (2015) e417.
25. L. Gao, H. Guo, L. Wei, C. Li, S. Gong and H. Xu, *Ceram. Int.*, 41 (2015) 8305.
26. P. Sokołowski, L. Pawłowski, D. Dietrich, T. Lampke and D. Jech, *Journal of Thermal Spray Technology*, 25 (2016) 94.
27. A.S.M. Ang and C.C. Berndt, *Surface & Coatings Technology*, 259 (2014) 551.
28. G. Witz, V. Shklover, W. Steurer, S. Bachegowda and H.P. Bossmann, *Surface & Coatings Technology*, 265 (2015) 244.
29. S. Govindarajan, R.O. Dusane and S.V. Joshi, *Journal of the American Ceramic Society*, 97 (2015) 3396.
30. L. Gao, L. Wei, H. Guo, S. Gong and H. Xu, *Ceram. Int.*, 42 (2016) 5530.
31. H. Wang, L.I. Zhijun, W. Tang, Y. Hao, I.T. Center and S. Polytechnic, *Transactions of the China Welding Institution*, 35 (2014) 41.
32. S. Miszczak, B. Pietrzyk and D. Kucharski, *Physica Status Solidi*, 213 (2016) 1109.
33. P. Carpio, M.D. Salvador, A. Borrell, E. Sánchez and R. Moreno, *Surface & Coatings Technology*, 307 (2016) 713.
34. M. Berni, N. Lopomo, G. Marchiori, A. Gambardella, M. Boi, M. Bianchi, A. Visani, P. Pavan, A. Russo and M. Marcacci, *Materials Science & Engineering C Materials for Biological Applications*, 62 (2016) 643.
35. P.J. He, S. Yin, C. Song, F. Lapostolle and H.L. Liao, *Journal of Thermal Spray Technology*, 25 (2016) 558.
36. N.I.D.A. Lopes, D.A.S. Leandro and V.T. Lopes Buono, *Advances in Science & Technology*, 97 (2016) 147.
37. M.F. Gong, F. Mei, S.R. Qiao, S.H. Wu and B.A. Lyashenko, *Surface Engineering*, 31 (2015)

1743294415Y.000.
38. N. Sanpo, J. Tharajak, J. Wang and C.C. Berndt, *Applied Mechanics & Materials*, 804 (2015) 104.
39. X.Q. Jin and C.Y. Zhao, *Ceram. Int.*, 41 (2015) 14915.
40. J.M. Tulliani, C. Bartuli, E. Bemporad, V. Naglieri and M. Sebastiani, *Ceram. Int.*, 35 (2009) 2481.
41. Y.J. Chang, A.P. Periasamy and S.M. Chen, *Int. J. Electrochem. Sc.*, 6 (2011) 4188.
42. Y. Yim, W. Hwang and S. Hwang, *Journal of The Electrochemical Society*, 142 (1995) 2604.
43. R. Moreno, J. Requena and J. Moya, *Journal of the American Ceramic Society*, 71 (1988) 1036.
44. I. Das, S.K. Medda, G. De, S. Fagerlund, L. Hupa, M.A. Puska and P.K. Vallittu, *Journal of the American Ceramic Society*, 98 (2015) 2428.
45. H.L. Huang, Y.Y. Chang, J.C. Weng, Y.C. Chen, C.H. Lai and T.M. Shieh, *Thin Solid Films*, 528 (2013) 151